



Cloud- and ice-albedo feedbacks drive greater Greenland Ice Sheet sensitivity to warming in CMIP6 than in CMIP5

Idunn Aamnes Mostue¹, Stefan Hofer^{1,2}, Trude Storelvmo¹, and Xavier Fettweis³

¹Department of Geosciences, University of Oslo, Oslo, Norway

²School of Geographical Sciences, University of Bristol, Bristol, United Kingdom

³Department of Geography, SPHERES research unit, University of Liège, Liège, Belgium

Correspondence: Idunn Aamnes Mostue (idunnam@uio.no)

Received: 10 February 2023 – Discussion started: 21 February 2023

Revised: 1 September 2023 – Accepted: 6 November 2023 – Published: 1 February 2024

Abstract. The Greenland Ice Sheet (GrIS) has been losing mass since the 1990s as a direct consequence of rising temperatures and has been projected to continue to lose mass at an accelerating pace throughout the 21st century, making it one of the largest contributors to future sea-level rise. The latest Coupled Model Intercomparison Project Phase 6 (CMIP6) models produce a greater Arctic amplification signal and therefore also a notably larger mass loss from the GrIS when compared to the older CMIP5 projections, despite similar forcing levels from greenhouse gas emissions. However, it is also argued that the strength of regional factors, such as melt–albedo feedbacks and cloud-related feedbacks, will partly impact future melt and sea-level rise contribution, yet little is known about the role of these regional factors in producing differences in GrIS surface melt projections between CMIP6 and CMIP5. In this study, we use high-resolution (15 km) regional climate model simulations over the GrIS performed using the Modèle Atmosphérique Régional (MAR) to physically downscale six CMIP5 Representative Concentration Pathway (RCP) 8.5 and five CMIP6 Shared Socioeconomic Pathway (SSP) 5-8.5 extreme high-emission-scenario simulations. Here, we show a greater annual mass loss from the GrIS at the end of the 21st century but also for a given temperature increase over the GrIS, when comparing CMIP6 to CMIP5. We find a greater sensitivity of Greenland surface mass loss in CMIP6 centred around summer and autumn, yet the difference in mass loss is the largest during autumn with a reduction of 27.7 ± 9.5 Gt per season for a regional warming of $+6.7^\circ\text{C}$ and 24.6 Gt per season more mass loss than in CMIP5 RCP8.5 simulations for the same warming. Assessment of the surface energy budget and

cloud-related feedbacks suggests a reduction in high clouds during summer and autumn – despite enhanced cloud optical depth during autumn – to be the main driver of the additional energy reaching the surface, subsequently leading to enhanced surface melt and mass loss in CMIP6 compared to CMIP5. Our analysis highlights that Greenland is losing more mass in CMIP6 due to two factors: (1) a (known) greater sensitivity to greenhouse gas emissions and therefore warmer temperatures and (2) previously unnotified cloud-related surface energy budget changes that enhance the GrIS sensitivity to warming.

1 Introduction

The Greenland Ice Sheet (GrIS) has been losing mass at an accelerating pace since the mid-1990s and is expected to continue to lose mass during the 21st century (Hanna et al., 2008; Fettweis et al., 2013; Mouginito et al., 2019; Noël et al., 2021; Doblus-Reys et al., 2021). Fluctuations in the mass balance occur with variations in glacial discharge, meltwater runoff, and accumulation of snow on the ice sheet surface. However, the recent mass loss is dominated by a reduction in the surface mass balance (SMB) along the edges of the ice sheet – the ablation zone – from surface melt (ME) and subsequent runoff (RU) from meltwater produced at the surface (van den Broeke et al., 2016; IMBIE2, 2020).

Due to the dark exposed bare ice during the summer melt season, melt in the ablation zone is mainly driven by absorbed solar radiation (Box et al., 2012; van den Broeke et al., 2008, 2017; Noël et al., 2019). The displacement of

mass from the ice sheet into the ocean contributes to global sea-level rise, threatening coastal ecosystems, human habitats, and livelihoods (Hauer et al., 2020; Doblus-Reys et al., 2021).

Clouds are of first-order importance in altering the GrIS energy budget, both in the long-wave (LW) radiative energy spectrum by absorbing and emitting LW and in the short-wave (SW) radiative energy spectrum by reducing the amount of the incoming SW and thus cooling the surface. There is thus a competing influence on the SW and LW radiative energy spectra from clouds over the GrIS, which can either warm or cool the surface (Shupe et al., 2004; Bennartz et al., 2013; van Tricht et al., 2016; Hofer et al., 2019).

Arctic amplification and circulation changes have been pointed out as the main drivers of the recent SMB loss from the GrIS (Tedesco et al., 2011, 2016; Bennartz et al., 2013; Fausto et al., 2016). While Arctic amplification leads to an anomalous increase in the near-surface temperatures (Screen and Simmonds, 2010), more frequent anticyclonic circulation conditions lead to a reduction in clouds (Hofer et al., 2017) and enhanced melt–albedo feedbacks (Tedesco et al., 2011; Box et al., 2012).

The latest Coupled Model Intercomparison Project (CMIP) Phase 6 models produce a greater Arctic amplification signal and therefore also a notably larger mass loss from the GrIS when compared to older CMIP5 projections, despite using nominally comparable forcing scenarios (O’Neil et al., 2016). CMIP6 models have also shown to project more Arctic precipitation compared to CMIP5 at the end of the 21st century (McCrystall et al., 2021), which can impact the surface albedo and further the surface mass balance (Box et al., 2022). However, a study by Hofer et al. (2020) showed that the rainfall projections between CMIP5 and CMIP6 regional climate model output over Greenland only start diverging from the year 2070 onward, whereas the surface mass balance starts to diverge from the year 2020 onward. In addition, the two model groups also have different regional feedbacks, such as melt–albedo feedback and cloud-related feedbacks, which will partly impact future melt and sea-level rise contribution by altering the energy available for melt at the surface. The difference in both Arctic warming levels and regional feedbacks will influence future mass loss. Yet, little is known about the relative importance of these regional factors when comparing CMIP6 to CMIP5 over Greenland.

In this study we analyse regional climate model outputs with the main focus on comparing future projections at a given warming level. In this way we can disentangle whether the differences in melt and mass loss come from a greater sensitivity at a given temperature or just from the fact that CMIP6 models warm more in absolute terms over Greenland and the Arctic.

2 Methods

2.1 Driving mechanisms of surface melt

Significant amounts of positive residual energy are needed for melt-induced surface mass loss over the GrIS (van den Broeke et al., 2008; Franco et al., 2013). Therefore, the analysis of this study focuses on the long-term changes in radiative surface energy budget (SEB) components over the ice sheet. With positive orientation downward to the surface, the balance can be described through Eq. (1), where a surplus in the SEB will give rise to surface melt (ME). The net long-wave radiation (LW_{net}) constitutes the long-wave radiation emitted downward to the surface (LWD) and from the surface (LWU). The net short-wave radiation (SW_{net}) depends on the incoming solar radiation at the top of the atmosphere (i.e. short-wave down – SWD); the surface albedo (α); and the influence of clouds, aerosols etc. on the transmissivity of the atmosphere (i.e. altering the amount of incoming SWD reaching the surface).

$$\begin{aligned} \text{ME} &= \text{LWD} - \text{LWU} + \text{SWD}(1 - \alpha) + \text{SHF} + \text{LHF} \\ &\quad + \text{GHF} \quad (\text{W m}^{-2}) \\ &= \text{LW}_{\text{net}} + \text{SW}_{\text{net}} + \text{SHF} + \text{LHF} + \text{GHF} \quad (\text{W m}^{-2}) \quad (1) \end{aligned}$$

The surface mass balance (SMB) defines the difference between accumulation (i.e. through precipitation – P) and ablation (i.e. through sublimation – SU , erosion of snow by wind – E , and meltwater runoff – RU) at the ice sheet:

$$\text{SMB} = \text{PR} - \text{SU} - E - \text{RU} \quad (\text{Gt yr}^{-1}). \quad (2)$$

In the interior of the GrIS – the accumulation zone – the snow pack is highly reflective of any incoming solar radiation (i.e. it has a high albedo), and so any variation in the absorbed energy budget over the accumulation zone is primarily controlled by the long-wave (LW) radiation fluxes (Charalampidis et al., 2015; van den Broeke et al., 2017).

In contrast to the high albedo in the accumulation zone, the ablation zone around the edges of the ice sheet experiences bare ice exposure during the summer melt; thus absorption of SWD is enhanced. Hence, in this area the surface energy budget is primarily controlled by short-wave (SW) radiation fluxes when bare ice is exposed during summer melt season (van de Wal et al., 2005; van den Broeke et al., 2011).

2.2 Data

For the analysis of this study we use data based on the same simulations as those that were used for segments of the work done by Hofer et al. (2020). They used a set of 11 high-resolution (15 km) regional climate model simulations over the GrIS. These simulations were conducted by using the regional climate model *Modèle Atmosphérique Régional* (MAR) to physically downscale six CMIP5 and five CMIP6

models (Eq. 1), using the Representative Concentration Pathway (RCP) 8.5 and Shared Socioeconomic Pathway (SSP) 5-8.5 high-emission scenarios respectively. Hofer et al. (2020) base their CMIP5 model selection on the Ice Sheet Model Intercomparison Project for CMIP6 (ISMIP6), fully described in Barthel et al. (2020). A “top three” CMIP5 model ensemble was selected following the ISMIP6 protocol (i.e. (i) the model must provide 6 h outputs as input to MAR at its lateral boundaries; (ii) the model must provide 6 h outputs for the RCP2.6 and RCP8.5 scenario projections; (iii) with regard to historical atmospheric, surface, and subsurface ocean metrics, the model must lie in the upper half of 33 model ensembles; and (iv) all climate change metrics of the model must lie within the two interquartile ranges of the multi-model median of the normalised projected change over Antarctica and Greenland). An additional three models were picked to maximise the projected diversity of the end of the century climate change projections, i.e. to capture the full diversity of the ensemble. Hofer et al.’s (2020) selection of the top CMIP6 models was limited by model availability at the time, with only 5 of the 17 available models meeting the first requirement of 6 h output. However, all five models were included in the CMIP6 model ensemble, as Hofer et al. (2020) found them to acceptably represent the model mean, minimum, and maximum of the full ensemble.

For this study we use the same 11 MAR simulations running from 1950 to 2100. However, in contrast to previous studies, we calculate different anomalies for various Greenland climate variables, i.e. near-surface temperature (2 m temperature), SMB, cloud cover, and SEB components based on the 1961–1990 mean state of each model simulation. The GrIS is assumed to have been in stable state during the 30-year period from 1961–1990 (van den Broeke et al., 2016), which is why this was chosen as our reference period. Furthermore, we focus on the physical drivers of enhanced GrIS mass loss in CMIP6 at a given level of warming, which have not been studied in detail before.

We use the anomalies for projecting any yearly or seasonal spatially averaged change over the GrIS surface for a given regional temperature increase and compare these projections produced by CMIP5 and CMIP6. These anomalies were calculated individually for each of the MAR simulations forced by the 11 global circulation models (GCMs), before being averaged over all six MAR simulations of CMIP5 models (hereafter MAR CMIP5) and over all five MAR simulations of CMIP6 models (hereafter MAR CMIP6). As the focus of our analysis is on the response and changes over the ice sheet area of Greenland only, we mask out every modelled pixel containing less than 10 % ice cover. With a 10 % ice cover mask that does not change over time, we expect our SMB reduction to be slightly overestimated compared to a dynamic ice mask, but recent research has indicated this error to be somewhere between 1 % and 6 % (Kjeldsen et al., 2020; Hansen et al., 2022).

Additionally, we look at a 20-year averaged period of $\sim 4^\circ\text{C}$ (2 m temperature) regional warming over Greenland to seek any potential differences in how changes in cloud cover, radiation, and surface mass flux variables are spatially distributed over the ice sheet in order to gain further insight into the spatial patterns of changes caused by rapid Greenland warming. The individual CMIP models warm at different rates and thus do not reach the same temperature by the end of the century. We therefore look at a threshold temperature to be able to compare all models for the same temperature increase. We decided on a 4°C warming as this is the highest temperature rise for a 20-year averaged period reached by all CMIP5 and CMIP6 models. These 20-year warming periods were calculated for a seasonal mean and for each of the 11 MAR simulations individually by creating a moving average, with a centred window of 20 years over the near-surface warming time series. This allowed us to compute the arithmetic mean along the time series, where a 20-year (± 10 years around each step) average for each year in the time series is returned. Then, by picking the year that returns a temperature closest to our designated near-surface temperature, we found the 20-year time interval for each model of similarly averaged warming (see Table S2 in the Supplement for an overview of the individual warming periods of each MAR simulation). After picking a 20-year warming period for each model, we averaged over all six MAR simulations of CMIP5 models and over all five MAR simulations of CMIP6 models separately.

2.3 Modèle Atmosphérique Régional

As most of the increase in melt occurs in the narrow ablation zone or through an expansion of the ablation zone, models used to project future changes in SMB must be able to represent the dynamics at the local spatial scale of this area. The Modèle Atmosphérique Régional (MAR) is a polar regional climate model. The grid extent, projection, and resolution of MAR have been adapted specifically to the GrIS, which makes it capable of capturing regional changes in the SMB over the ice sheet (Fettweis et al., 2011, 2017). For this study, we use MARv3.9.6, previously evaluated by Delhasse et al. (2020). MAR is a hydrostatic primitive-equation model, consisting of a three-dimensional atmospheric model, coupled to a one-dimensional energy-balance-based surface and vegetation model, Soil Ice Snow Vegetation Atmospheric Transfer (SISVAT) (Gallee and Schayes, 1994; De Ridder, 1998; Fettweis et al., 2013). SISVAT models the exchange between the atmosphere and surface. It is multilayered and subdivided into a soil–vegetation module and a snow–ice module, where the latter is based on the snow model CROCUS (Brun et al., 1992; Vionnet et al., 2012).

The MAR Greenland setup covers an integration domain stretching from a 5.1°W – 88.4°W longitudinal extent and 54.89°N – 85.92°N latitudinal extent (see Fig. S1 in the Supplement). A 15×15 km spatial resolution was used, covering

Table 1. Forcing fields used to perform MAR simulations, historical periods and future scenarios of the simulations, and CMIP phase.

Forcing fields	Historical simulation	Future scenario	CMIP phase
ACCESS1.3	historical (1850–2005)	RCP8.5	5
CSIRO-Mk3-6-0	historical (1850–2005)	RCP8.5	5
HadGEM2-ES	historical (1850–2005)	RCP8.5	5
IPSL-CM5A-MR	historical (1850–2005)	RCP8.5	5
MIROC5	historical (1850–2005)	RCP8.5	5
NorESM1-M	historical (1850–2005)	RCP8.5	5
CESM2	historical (1850–2014)	SSP5-8.5	6
CNRM-CM6-1	historical (1850–2014)	SSP5-8.5	6
CNRM-ESM2-1	historical (1850–2014)	SSP5-8.5	6
MRI-ESM2-0	historical (1850–2014)	SSP5-8.5	6
UKESM1-0-LL	historical (1850–2014)	SSP5-8.5	6

a domain of 210×115 (latitude, longitude) grid points. The MAR Greenland setup was run with a vertical resolution of 24 pressure-ratio levels, with the model top pressure set at 0.1 hPa. A 6-hourly input of specific humidity, u and v wind components, and temperature and sea-level pressure, as well as a daily input of sea-surface temperature and concentration, was provided at the lateral boundaries of MAR.

For the simulations used in this study, MAR was run in “community mode”, meaning that a member is started every 5 years over 1950–2090 and initialised by the snowpack simulated for the beginning (i.e. 1 September) of the 15-year simulated periods by the former MARv3.9 based on simulations using the same GCM as forcing. As the period simulated by each member covers at least two members initialised at different years (5 and 10 years ago), the retained years of each member were chosen to be independent of the initial conditions, i.e. to have a difference in SMB and runoff as well as refreezing lower than 1 GT yr^{-1} , between the different members for the same year. Due to the high liquid water content allowed in MAR, a snowpack can quickly lose (~ 10 years) its capacity to retain meltwater as it becomes too dense. Further, these simulations resolve the first 30 m of snow. A layer is automatically added/removed at the bottom if the total snow is $< 29 \text{ m}$ or $> 314 \text{ m}$. The maximum liquid water content in MAR is 7% (Lefebvre et al., 2003).

Finally, the MAR model physics and resolution remained unchanged across the downscaling for all 11 GCMs.

3 Results

3.1 GrIS surface mass balance change

Annual summer (JJA) and autumn (SON) seasonal SMB, melt, and runoff anomalies (Gt per season) are presented in Fig. 1 as functions of near-surface temperature anomalies ($^{\circ}\text{C}$) over the GrIS. In the year 2100 we observe that MAR CMIP6 temperatures extend beyond those of MAR CMIP5 on the x axis, yielding a $+1.4^{\circ}\text{C}$ greater warming over the

GrIS than in MAR CMIP5 annually ($+1.8^{\circ}\text{C}$ in summer and autumn). Consequently, MAR CMIP6 reaches a higher melt (pink) and runoff (purple) anomaly and subsequently a greater surface mass loss (green), partly due to a higher near-surface temperature anomaly than what is found for MAR CMIP5. However, we also find a greater sensitivity of the GrIS SMB reduction in MAR CMIP6, even when looking at the same warming. In Fig. 1a we see that MAR CMIP6 projects a higher annual melt and runoff anomaly for a given warming and subsequently a greater surface mass loss (SMB; green) when compared to MAR CMIP5. This clearly suggests that parts of the greater mass loss in MAR CMIP6 over the GrIS are driven by a difference in SMB sensitivity for a given temperature change between the ensembles.

Due to the geographical position of Greenland, the timing of the melt season is closely connected to the seasonal changes in solar radiation (Fettweis et al., 2011), and we expect most of the surface melt to occur over the 3 summer months of June, July, and August (JJA). We observe in Fig. 1b the largest absolute contribution of melt, runoff, and SMB reduction during summer for both MAR CMIP5 and MAR CMIP6 in a warming climate. Conversely, in Fig. 1c we find that the largest difference in projected melt, runoff, and SMB between MAR CMIP5 and MAR CMIP6 occurs in autumn. Here, MAR CMIP6 projects a surface mass loss reduction of $27.7 \pm 9.5 \text{ Gt}$ per season for a temperature increase of $+6.7^{\circ}\text{C}$ (see Table S1 in the Supplement) and 24.6 Gt per season more mass loss than MAR CMIP5 at the same temperature increase (see Table S1). For winter (DJF; Fig. S2) and spring (MAM; Fig. S3) the difference in SMB between MAR CMIP5 and MAR CMIP6 is negligible and is not discussed further. This suggests that the main driver of the greater mass loss sensitivity in MAR CMIP6 compared to MAR CMIP5 in the annual mean stems from the difference in sensitivity in autumn.

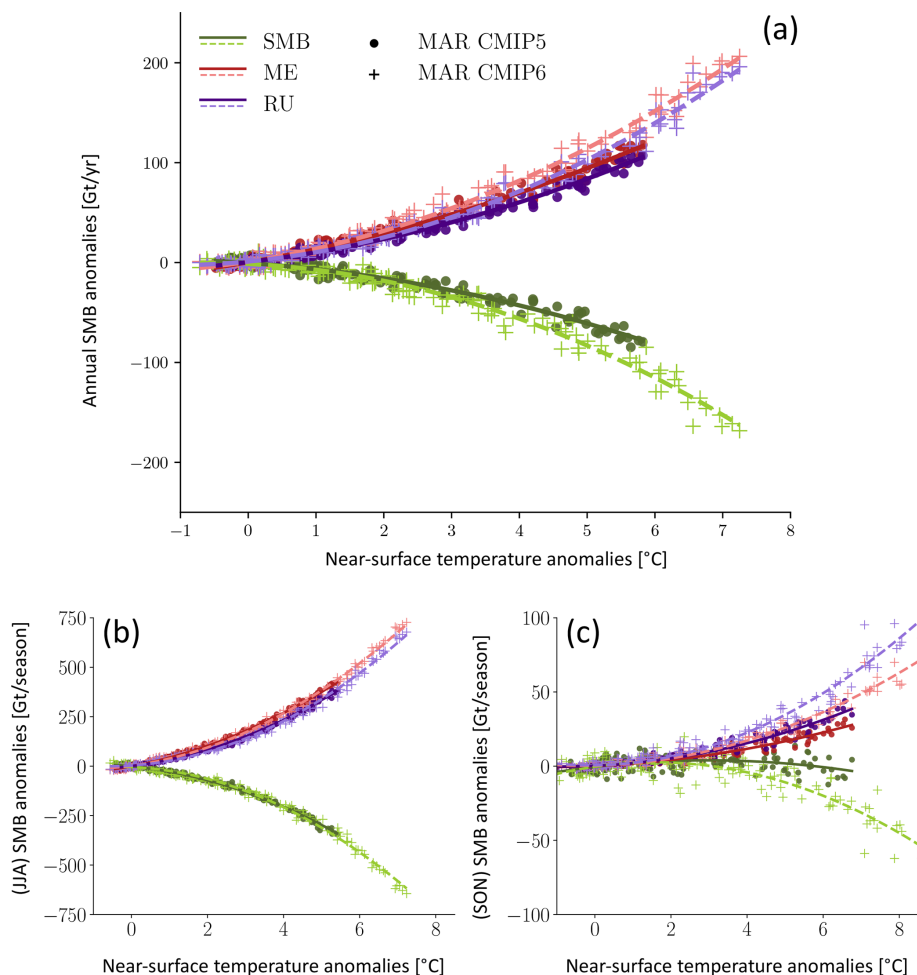


Figure 1. SMB, melt, and runoff anomalies (Gt yr^{-1}) over the GrIS as a function of near-surface temperature anomalies ($^{\circ}\text{C}$) in Greenland. **(a)** Annual SMB, melt (ME), and runoff (RU) anomalies (Gt yr^{-1}) over the GrIS as a function of annual near-surface temperature anomalies ($^{\circ}\text{C}$) over Greenland from MAR CMIP5 (dots) and MAR CMIP6 (crosses), with regression drawn in solid lines for MAR CMIP5 and dashed lines for MAR CMIP6. All anomalies are related to the 30-year averaged reference period (1961–1990). Panels **(b)** and **(c)** are the same as panel **(a)** but for a seasonal mean of summer and autumn respectively.

3.2 Cloud contribution to surface energy budget change

To assess where the difference in SMB for a given warming between MAR CMIP5 and MAR CMIP6 comes from, we analyse the radiative energy available for melt at the surface over the GrIS in summer and autumn (sensible and latent heat fluxes have also been studied in Fig. S4 but are shown to be insignificant). We observe a similar general behaviour of the radiative SEB components (i.e. net short wave – SW_{net} , downwelling short wave – SWD, net long wave – LW_{net} , downwelling long wave – LWD, and upwelling long wave – LWU) with warming temperatures from MAR CMIP5 and MAR CMIP6 over both summer (Fig. 2a) and autumn (Fig. 2b). Here, the SW_{net} (orange) reaching the surface increases with warming – an effect that seems to be coming from the melt–albedo feedback and darkening of the surface

– despite decreasing SWD (purple), concurrent with the increase in LWD (red). However, while we observe similar behaviour of the projection of SEB components between MAR CMIP5 and MAR CMIP6 in autumn (Fig. 2b), differences are found between the two ensembles in summer (Fig. 2a).

Although the net radiative flux (grey) behaves similarly for MAR CMIP5 and MAR CMIP6 for a given near-surface temperature increase in summer (Fig. 2a), the short- and long-wave components composing the net radiative flux show different behaviours between the two ensembles for this season. We observe that there is more SW_{net} radiation reaching the surface in MAR CMIP6 compared to MAR CMIP5 for a given warming, which mainly comes from more SWD reaching the surface in MAR CMIP6. Further, we observe less net long-wave flux (LW_{net} ; blue) absorbed at the surface in MAR CMIP6 compared to MAR CMIP5. The amount of outgoing long-wave radiation emitted from the surface (LWU; green)

behaves similarly between the two ensembles, so the difference we observe in LW_{net} comes from a decrease in downwelling long-wave radiation (LWD; red) for a given temperature increase in MAR CMIP6.

The difference in summer LWD and SWD is indicative of an effect from a change in cloud properties (i.e. cloud cover and cloud optical depth; COD), affecting the transmissivity and emissivity of the atmosphere. In terms of cloud cover, MAR CMIP5 and MAR CMIP6 show a diverging behaviour over both seasons (Fig. 2c, d). While the magnitude of the changes in cloud cover in summer is the same between MAR CMIP5 and MAR CMIP6 with warming, we see completely different behaviours in terms of the sign of the change (Fig. 2c). In MAR CMIP5 cloud cover increases ($+2.4 \pm 0.9\%$) with warming ($+5.4^\circ\text{C}$), while in MAR CMIP6 cloud cover over the GrIS notably decreases ($-2.2 \pm 1.1\%$) for a given warming ($+5.4^\circ\text{C}$, Fig. 2c; see Table S1). The decrease in cloud cover explains why we also see more SWD reaching the surface in summer in MAR CMIP6 compared to MAR CMIP5 (Fig. 2a) as the transmissivity of the atmosphere increases with decreasing cloud cover. Moreover, the magnitude of the difference is not as pronounced in autumn as in summer. In autumn, there is an increase in cloud cover of $+2.9 \pm 0.8\%$ in MAR CMIP5 and a decrease of $-0.7 \pm 0.9\%$ in MAR CMIP6 for a $+6.7^\circ\text{C}$ near-surface warming (Fig. 2d; see Table S1).

We suggest the higher amount of SWD reaching the surface of the GrIS in MAR CMIP6 is primarily a consequence of the decrease in cloud cover with warming during summer. Because we do not see major differences in cloud optical depth (Fig. 3a), we can likely rule out a notable contribution from changes in cloud microphysics between MAR CMIP5 and MAR CMIP6 over Greenland (i.e. water-phase changes) in summer.

Conversely, in autumn (Fig. 3b) there is a small difference in COD anomaly (Fig. 3b). We see an increase of $+0.8 \pm 0.01$ in MAR CMIP5 and $+0.1 \pm 0.01$ in MAR CMIP6 for a $+6.7^\circ\text{C}$ near-surface temperature warming (see Table S1). In autumn, the data therefore suggest that optically thicker clouds counteract the effect of cloud cover reduction in MAR CMIP6 (Fig. 2d). Therefore, we observe no difference in the autumn SW and LW radiative energy (Fig. 2b) between MAR CMIP5 and MAR CMIP6 that can explain the difference in the autumn SMB (Fig. 1c).

We have also studied the radiative surface energy flux and cloud cover change for the GrIS ablation zone and accumulation zone individually. We provide methods and results in Figs. S17 and S18.

3.3 Spatial distribution over the GrIS

We have observed how the spatially averaged GrIS surface mass and energy balance components change on long timescales. However, as the spatial distribution of the SEB, and therefore also the SMB, over the GrIS is not uniform, we

further explore the spatial change in cloud cover, its effect on the radiative budget at the surface, and finally the SMB response for a 20-year warming period ($+4^\circ\text{C} \pm 10$ years) compared to a 30-year averaged reference period (1960–1990).

3.3.1 Cloud cover

The different cloud cover responses over the GrIS in summer (JJA; Fig. 4) project spatially homogeneous patterns. While we observe an overall increase in total cloud cover in MAR CMIP5 with warming over most of the GrIS in summer, we see a general decrease in MAR CMIP6. Due to the homogeneous nature of the difference between MAR CMIP6 and MAR CMIP5 (JJA, CMIP6–CMIP5), we argue that differences in circulation are unlikely to be the driver behind this difference in cloud cover response with warming, as circulation-driven cloud cover change would be expected to result in a more distinct spatial pattern in areas with anomalous upslope and downslope winds. Additionally, the data also suggest that this pattern in cloud cover stems mostly from a contrasting behaviour in upper-level clouds (< 440 hPa), while mid-level clouds (≥ 440 hPa, ≤ 680 hPa) and low-level clouds (> 680 hPa) do not behave very differently (see Fig. S3 for JJA mid- and low-level clouds). We expect this homogeneous pattern of cloud cover reduction in MAR CMIP6 to lead to a greater proportion of short-wave radiation reaching large parts of the surface of the GrIS in summer in MAR CMIP6.

In autumn (SON) we detect similar patterns of cloud cover trends with warming between MAR CMIP5 and MAR CMIP6 (Fig. 4) but of different magnitudes. In the total cloud cover, MAR CMIP5 shows increasing cloud cover over most regions of the ice sheet, with an exception of modest decrease over the extreme south-east. In the north-west area where MAR CMIP5 shows its strongest positive cloud cover anomaly, MAR CMIP6 only shows a modest increase, whereas the rest of the ice sheet experiences a decrease in cloud cover. We also see more negative cloud cover anomalies over the whole ice sheet in MAR CMIP6 when compared to MAR CMIP5 (SON, CMIP6–CMIP5). Again, the data also suggest for the autumn clouds that this pattern in cloud cover stems mostly from a contrasting behaviour in upper-level clouds, while mid- and low-level clouds do not behave very differently (see Fig. S4 for SON mid- and low-level clouds).

In Figs. S13 and S14 we show in detail the cloud cover response for each of the six CMIP5 models and five CMIP6 models respectively where the individual models (except MIROC5) generally capture the ensemble mean well. Therefore, we argue that the models chosen for downscaling capture the overall cloud cover response for CMIP5 and CMIP6.

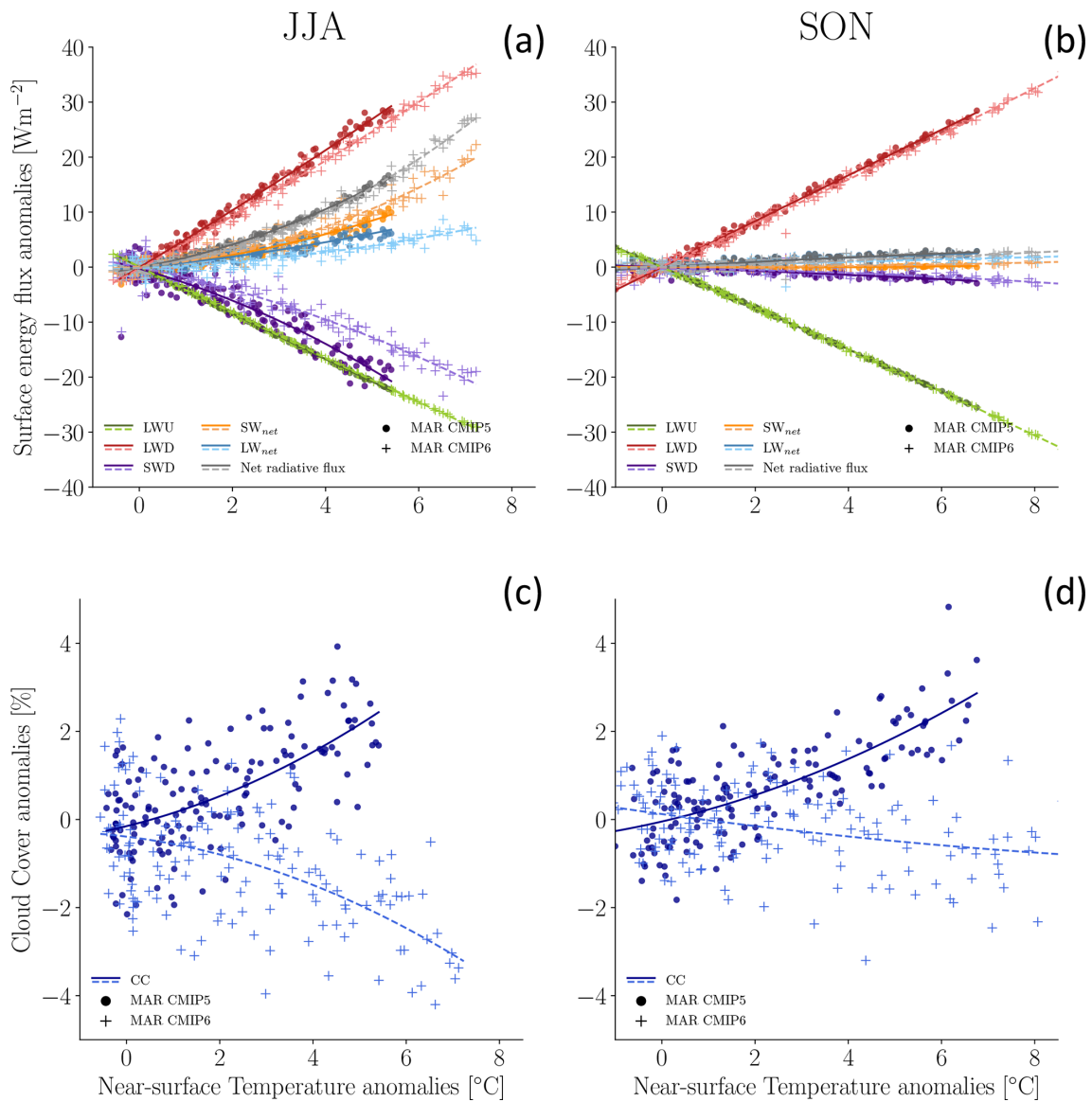


Figure 2. Radiative SEB component anomalies ($W m^{-2}$) and total cloud cover anomalies (%) as a function of the near-surface air temperature anomalies ($^{\circ}C$). **(a)** Seasonal (JJA) radiative SEB component anomalies ($W m^{-2}$) over the GrIS according to near-surface air temperature anomalies ($^{\circ}C$) from MAR CMIP5 (dots) and MAR CMIP6 (crosses), with regression drawn in solid lines for MAR CMIP5 and dashed lines for MAR CMIP6. It includes the radiative energy fluxes of long-wave down (LWD), long-wave up (LWU), short-wave down (SWD), net long-wave radiation (LW_{net}), net short-wave radiation (SW_{net}), and net radiative flux. There is a positive direction towards the surface. Panel **(b)** is the same as **(a)** but for autumn (SON). Panel **(c)** is the same as **(a)** but for the variable of cloud cover (%). Panel **(d)** is the same as **(c)** but for autumn (SON).

3.3.2 Radiative surface energy budget

Figure 5 shows the difference between the MAR CMIP6 anomaly and MAR CMIP5 anomaly of the radiative SEB components for summer (JJA; left) and autumn (SON; right) (see Figs. S5 and S6 for individual MAR CMIP5 and MAR CMIP6 model mean anomalies for JJA and SON respectively). Hereafter, a lower anomaly means that there is a more negative MAR CMIP6 anomaly compared to the MAR

CMIP5 anomaly, and similarly a higher anomaly refers to a more positive MAR CMIP6 anomaly compared to the MAR CMIP5 anomaly.

In summer (JJA; Fig. 5), there is a lower downwelling LW radiative flux (LWD) anomaly and a higher downwelling SW radiative flux (SWD) anomaly over most of the ice sheet. This corresponds to what we expect from the homogeneous cloud cover reduction in summer in MAR CMIP6, increasing the transmissivity of the atmosphere. Moreover, there is an

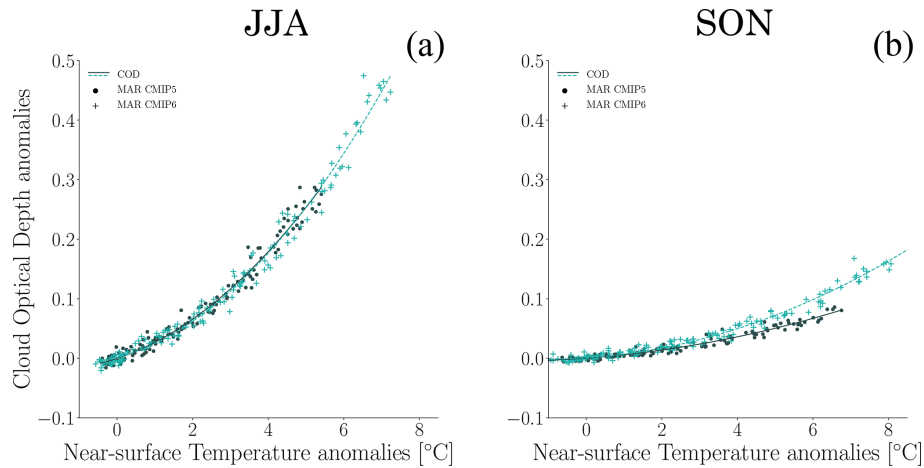


Figure 3. (a) Summer (JJA) cloud optical depth (COD) anomalies over the GrIS as a function of annual near-surface temperature anomalies ($^{\circ}\text{C}$) from MAR CMIP5 (dots) and MAR CMIP6 (crosses), with regression drawn in solid lines for MAR CMIP5 and dashed lines for MAR CMIP6. All anomalies are related to the 30-year average reference period (1961–1990). Panel (b) is the same as (a) but for autumn (SON).

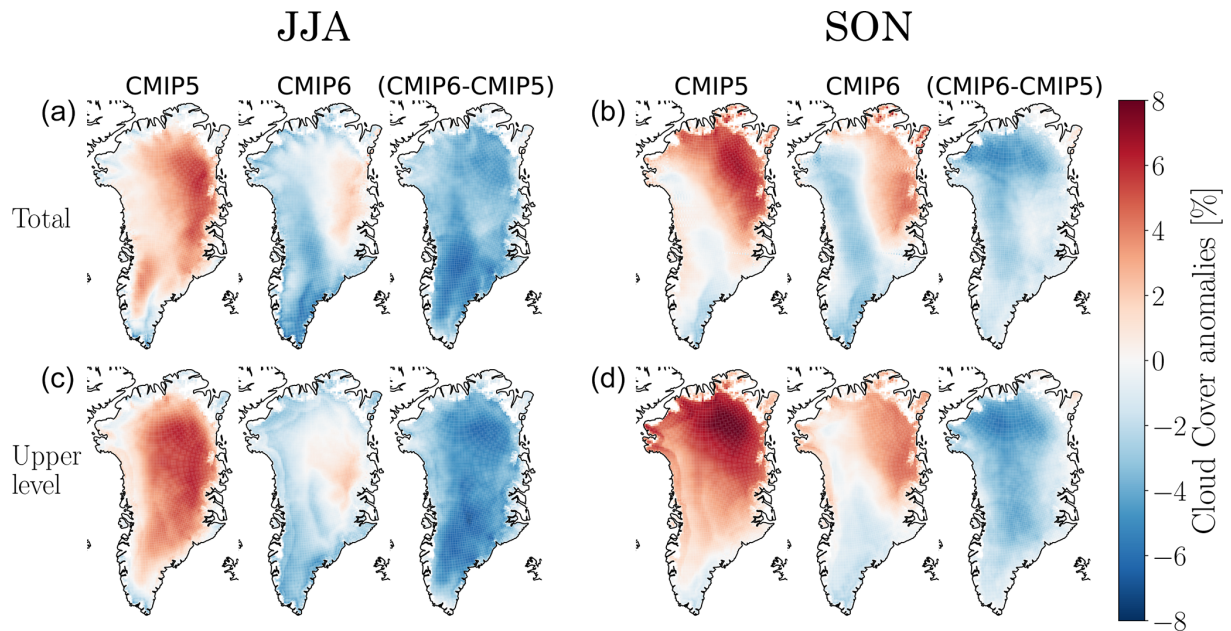


Figure 4. Cloud cover anomalies (%) for MAR CMIP5 and MAR CMIP6 simulations ($+4^{\circ}\text{C} \pm 10$ years) for summer (JJA) and autumn (SON). The 20-year average ($4^{\circ}\text{C} \pm 10$ years) of the cloud cover (%) over the GrIS for summer (JJA; **a**, **c**) and autumn (SON; **b**, **d**). The two rows indicate the total (**a**, **b**) and upper-level cloud cover (< 440 hPa, **c**, **d**). Each season has three columns – the first indicates the cloud cover anomalies for MAR CMIP5, the second indicates the cloud cover anomalies for MAR CMIP6, and the third indicates the difference between the two (CMIP6–CMIP5). For MAR CMIP5 and MAR CMIP6 a positive value (red) indicates an increase in cloud cover and a negative value (blue) a reduction in cloud cover compared to the reference period. For the difference (CMIP6–CMIP5) a positive value (red) indicates a more positive cloud cover anomaly, and negative values (blue) indicate a more negative cloud cover anomaly in MAR CMIP6 compared to MAR CMIP5.

overall lower LW_{net} radiation anomaly over the GrIS. With smaller amounts of LWD radiative flux over the GrIS from a reduction in cloud cover, we expect there to be less heat trapped, hence less warming of the snowpack from LW radiation. Further, because there was an overall increase in SWD radiation over the ice sheet, we have a higher SW_{net} radia-

tion anomaly in MAR CMIP6 concentrated along the edges where we find the dark ablation zone. We also see an interesting band of a slightly lower SW_{net} anomaly just above the ablation zone. We suspect this pattern to stem from the influence of reduced cloud cover over an area where clouds usually warm the highly reflective surface, i.e. less clouds

cool the surface. Therefore, due to a reduction in clouds in MAR CMIP6, the net energy flux is reduced above the ablation zone, leading to less melt over the bright surface and therefore a less pronounced melt–albedo feedback, causing a reduction in absorbed short-wave radiation in MAR CMIP6. Over the whole accumulation zone the snowpack will usually reflect more of the incoming SW radiation, and a reduction in cloud cover therefore leads to a cooling of the snowpack as a result of less LW_{net} radiation. Conversely, in the darker ablation zone where more bare ice is exposed, more of this extra SWD radiation in MAR CMIP6 can be absorbed, which leads to more melt or warming of the surface.

In autumn (SON; Fig. 5), there is a lower LWD anomaly over most of the GrIS, with an exception along the east coast where the anomaly is modestly higher. As for summer, there is an overall lower LW_{net} radiation anomaly across the whole ice sheet but of a smaller magnitude. A modestly higher SWD anomaly is also seen across most of the ice sheet, however slightly less in the extreme south-east. Therefore, we suggest the higher SW_{net} radiation anomalies – mostly centred around the southern ablation zone – come from a darker surface created in summer and the fact that they are still being exposed over the lower ablation zone during autumn. We expect this change in SW radiation around the lower ablation zone to enhance autumn melt and runoff over the lower ablation zone.

3.3.3 Surface mass balance response

Figure 6 shows the difference between the MAR CMIP6 anomaly and MAR CMIP5 anomaly of SMB, melt, runoff, and refreezing for summer (JJA; left) and autumn (SON; right) (see Figs. S7 and S8 for individual MAR CMIP5 and MAR CMIP6 model mean anomalies for JJA and SON respectively). Again, a lower anomaly means that there is a more negative MAR CMIP6 anomaly compared to the MAR CMIP5 anomaly, and similarly a higher anomaly refers to a more positive MAR CMIP6 anomaly compared to the MAR CMIP5 anomaly.

In summer, there is a lower SMB anomaly over most of the ablation zone and a higher SMB anomaly in the transition zone between the ablation zone and the accumulation zone (i.e. the percolation zone). The more negative SMB in MAR CMIP6 (relative to MAR CMIP5) appears to be coming from a higher melt and runoff anomaly in the same area, most likely induced by more absorbed SW radiation. Conversely, in the percolation zone we note an effect of a higher refreezing anomaly and subsequent lower runoff anomaly in MAR CMIP6, yielding the higher SMB anomaly for this area. Most likely, despite enhanced SW radiation due to less clouds, the simultaneous decreased incoming LW radiation reduces the bare ice exposure in the percolation zone where the residual snowpack is usually thicker and reflects sunlight more efficiently for longer. Thus, the ice sheet experiences less melt and runoff and more refreezing in this area during summer.

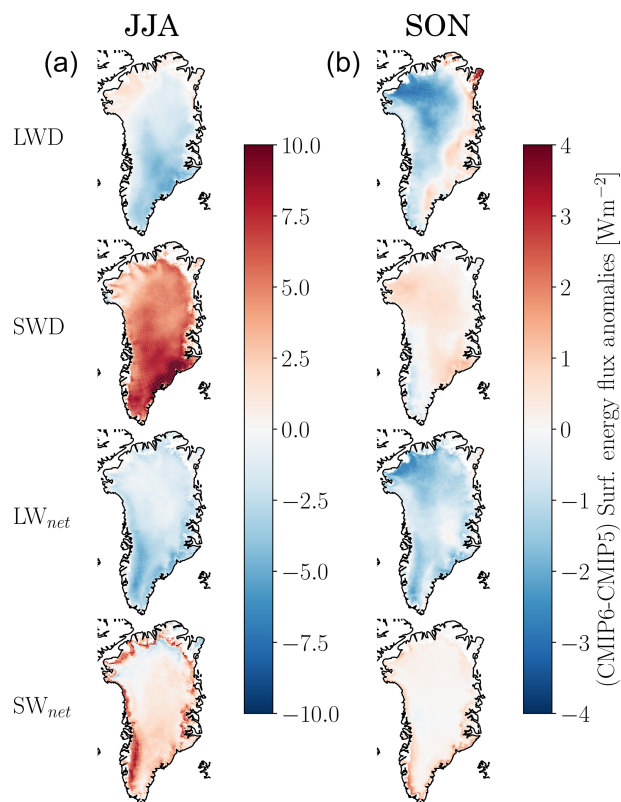


Figure 5. Difference in the anomaly of SEB fluxes between MAR CMIP6 and MAR CMIP5 simulations ($+4\text{ }^{\circ}\text{C} \pm 10$ years) for summer (JJA) and autumn (SON). The 20-year average ($+4\text{ }^{\circ}\text{C} \pm 10$ years) difference in SEB. The two columns indicate the mean difference in the anomalies for summer (a) and autumn (b). Positive values (red colours) indicate a greater energy flux reaching the surface in MAR CMIP5 compared to MAR CMIP6, whereas negative values (blue colours) indicate a smaller energy flux reaching the surface in MAR CMIP6 compared to MAR CMIP5. The colour bars in summer and autumn are not in the same range. See Fig. S15 for relative change plots.

The effect of the lower SMB anomaly in the ablation zone appears to cancel the effect of the higher SMB anomaly over the percolation zone; thus no difference is detected between MAR CMIP6 and MAR CMIP5 in the spatially averaged SMB projection with warming in summer (Fig. 1b).

In autumn we do not see the same buffering effect of more refreezing in MAR CMIP6 in the percolation zone as we saw in summer, partly due to a decrease in meltwater production in this region. Figure 6 shows a lower SMB anomaly mostly over the ablation zone, concentrated around the southern tip of the ice sheet. Over the lower parts of the ablation area in the south of the ice sheet we also see higher melt and runoff anomalies. The excess SWD reaching the surface in MAR CMIP6 in summer induces a stronger surface darkening of the lower ablation zone (shown in Fig. 7 in the following section), thus enhancing the surface mass loss in autumn where the bare ice is still exposed. With a reduced buffering effect

of refreezing in the percolation zone, compared to summer, we then detect a total difference in the spatially averaged autumn SMB from more melt and runoff in the darker ablation zone.

Parts of the refreezing in the percolation zone in MAR CMIP6 can possibly be explained by the faster warming pace of the CMIP6 ensemble (not shown). Different warming rates imply that “faster-warming” models (i.e. those of the 20-year period of $\sim 4^\circ\text{C}$ warming; see Table S2) have not had the same time to fully extend the ablation zone to higher elevations to the same extent as the other models that reach the same atmospheric temperature at a later stage. In the “slower-warming” models the ablation zone is more in equilibrium with the warming climate and therefore likely already larger in CMIP5 than in CMIP6 at a given warming because CMIP6 generally warms faster. This could explain parts of the higher refreezing in the percolation zone because CMIP5 might already have gotten rid of the buffering snow layer.

3.4 Melt–albedo feedback response

Future changes in the strength of the melt–albedo feedback play a leading part in how much energy is available for melt over the GrIS surface. We detect a decrease in the spatially averaged albedo anomaly as a function of increasing seasonal near-surface temperature for both MAR CMIP5 and MAR CMIP6 in summer (Fig. 7a), well known as a melt–albedo feedback. However, there is no difference in the spatially averaged albedo anomalies between MAR CMIP5 and MAR CMIP6, but the differences in the spatial summer distribution between MAR CMIP5 and MAR CMIP6 (Fig. 7c) show a lower albedo anomaly in the ablation zone around the ice sheet for MAR CMIP6, with the exception of the southeast coast. We believe this darkening of the surface is due to more SW radiative fluxes of bare ice over the ablation zone, induced from decreasing cloud cover in MAR CMIP6. This surplus of SW radiation in MAR CMIP6 leads to more melt over the dark ablation zone, enhancing surface darkening.

Conversely, we observe more positive anomalies over parts of the percolation zone in MAR CMIP6 compared to MAR CMIP5 (see Figs. S9 and S10 for individual MAR CMIP5 and MAR CMIP6 model mean anomalies for JJA and SON respectively). We suspect that parts of the percolation zone in MAR CMIP6 experience a surface cooling as a result of less LW radiation reaching the surface, stemming from the reduction in cloud cover. Therefore, this layer has a higher albedo because there is winter snow in this area that has experienced less long-lasting melt events in MAR CMIP6. We suggest that the more negative albedo anomaly detected in the ablation zone cancels out the more positive albedo in the percolation zone; thus there is no difference in the spatially averaged projection of the albedo between MAR CMIP6 and MAR CMIP5 in summer.

A general decrease in albedo anomalies with increasing near-surface temperature is also detected for both MAR

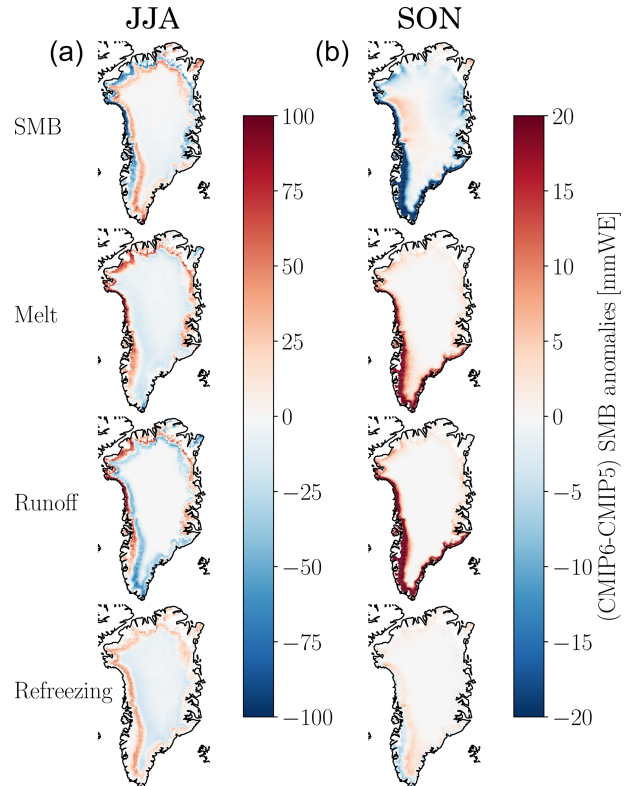


Figure 6. Difference in the anomaly of selected SMB components between MAR CMIP6 and MAR CMIP5 simulations ($+4^\circ\text{C} \pm 10$ years) for summer (JJA) and autumn (SON). The 20-year average ($+4^\circ\text{C} \pm 10$ years) difference in anomalies of melt, runoff, refreezing, and the total SMB (mm WE) of MAR (CMIP6–CMIP5). Anomalies are related to the reference period (1961–1990). The two columns indicate the mean difference in the anomalies for the summer season (JJA; **a**) and the autumn season (SON; **b**). Positive values (red) indicate a greater mass balance at the surface in MAR CMIP6 compared to MAR CMIP5, while negative values (blue) indicate a lower mass balance in MAR CMIP6 compared to MAR CMIP5. The colour bars in summer and autumn are not in the same range. See Fig. S16 for relative change plots.

CMIP5 and MAR CMIP6 in autumn (Fig. 7b). Here, MAR CMIP5 projects a decrease in albedo of -0.008 ± 0.001 and MAR CMIP6 a decrease of -0.014 ± 0.001 for a temperature increase of $+6.7^\circ\text{C}$ (see Table S1). The spatial distribution reveals a more negative albedo anomaly in MAR CMIP6 compared to MAR CMIP5 around the outer ablation zone (Fig. 7d). This lower albedo in autumn in MAR CMIP6 is likely due to the fact that the higher ablation zone first becomes covered with snow during autumn. However, the lower ablation zone experiences more melt and runoff in summer due to less clouds and therefore is darker coming into autumn. Here, the bare ice is still exposed in the lower ablation zone, leading to more absorption of SW radiation and surface melt in autumn, without a buffering effect from extra refreezing that we observed in summer.

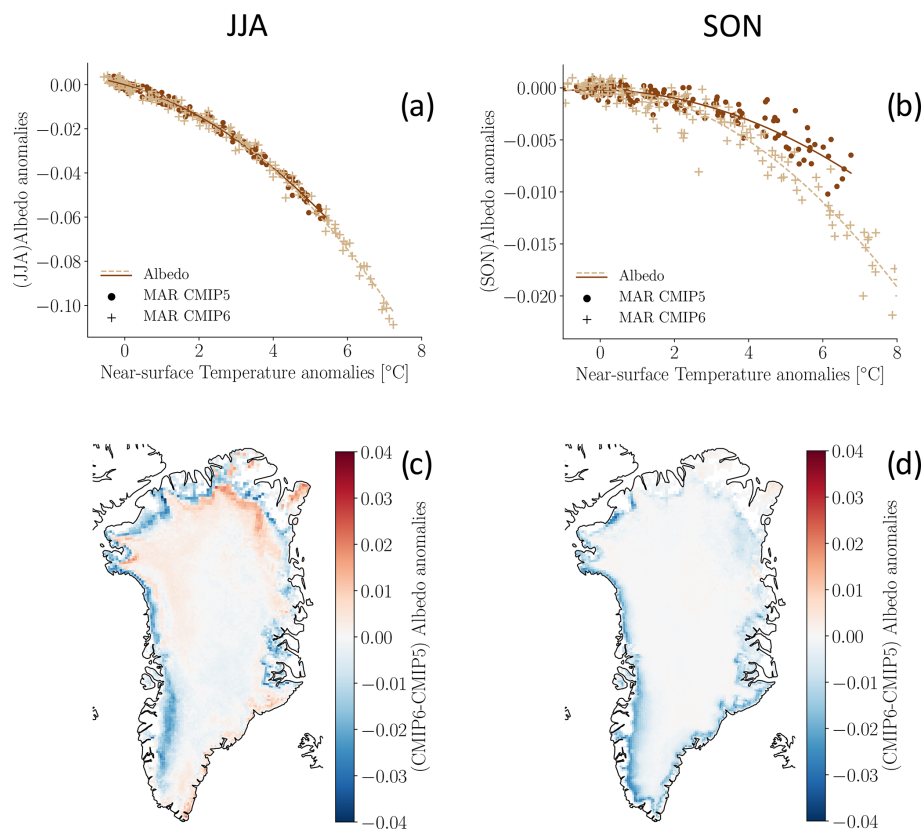


Figure 7. Albedo anomalies as a function of near-surface air temperature anomalies ($^{\circ}\text{C}$) over GrIS and spatial distribution for a warming period of 4°C . Seasonal albedo anomalies according to seasonal near-surface temperature ($^{\circ}\text{C}$) (a, b) and spatially distributed difference in change over GrIS for 4°C warming (c, d) for the summer season (JJA) (a, c) and autumn season (SON) (b, d). For the spatial maps, areas of positive values (red colours) indicate higher values of albedo, and negative values indicate lower values of albedo in MAR CMIP6 when compared to MAR CMIP5.

4 Discussion and conclusion

In this study, we performed an analysis of high-resolution regional climate model simulations over the GrIS to investigate possible physical mechanisms driving the excess SMB loss in CMIP6 models. Prior to this study, it has been believed that the excess SMB reduction seen in CMIP6 compared to CMIP5 was solely a product of a greater Arctic amplification signal in CMIP6 models. Our work suggests that part of the greater mass loss in CMIP6 over the GrIS is driven by a difference in SMB sensitivity from a change in cloud representation in CMIP6 models.

By comparing two model ensembles of six CMIP5 RCP8.5 and five CMIP6 SSP5-8.5 future projections for a given temperature increase, we found a greater sensitivity of Greenland surface mass loss in CMIP6 in summer and autumn. Yet, the difference in mass loss between CMIP5 and CMIP6 was the largest during autumn.

Assessment of future changes in the SEB and cloud properties over the GrIS suggested a reduction in high clouds during summer and autumn to be the main driver of additional SW radiation reaching the surface in CMIP6, while

cloud cover increases with warming in CMIP5. However, the detailed mechanisms behind different cloud cover trends with warming in CMIP6 compared to CMIP5 are still unknown. We suggest that future studies look in more detail into the circulation in both CMIP5 and CMIP6 over Greenland, although initial analysis suggests no notable difference between the two ensembles (Delhasse et al., 2020).

The impact of a reduction in cloud cover on the radiative energy budget and SMB over the GrIS is schematically represented in Fig. (8). Our data showed a stronger melt–albedo feedback in CMIP6 mainly in the lower ablation zone where bare ice is continuously exposed during summer and early autumn. Here we observed more surface melt and darkening of the surface during summer due to an increase in SWD from reduced cloud cover (Fig. 8a–b). However, because of a competing mechanism in the percolation zone leading to more refreezing (Fig. 8a–b), there was no difference in the total SMB projection between CMIP5 and CMIP6 in summer. In autumn, however, there was a stronger melt and runoff signal in CMIP6 due to the darkening of the lower albedo zone in summer (Fig. 8c–d).

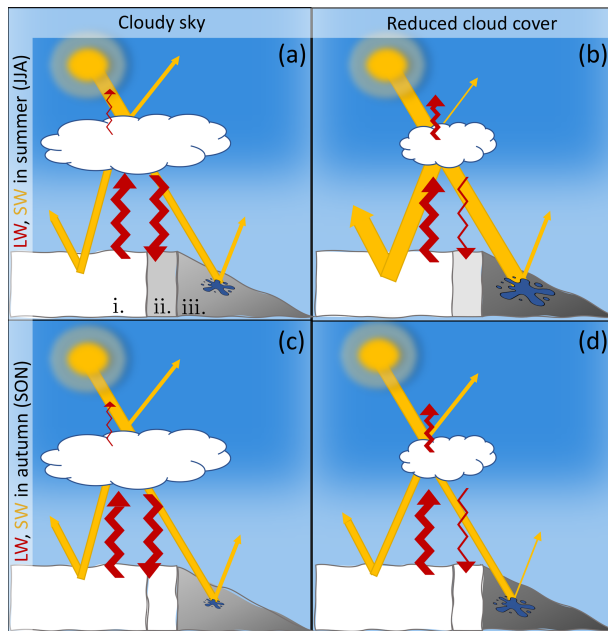


Figure 8. Schematic radiative energy flows over the GrIS in CMIP5 (cloudy sky) and CMIP6 (reduced cloud cover). Simplified schematic representation of the radiative energy flows over the Greenland Ice Sheet for cloudy sky conditions (a, c) and reduced cloud conditions (b, d), for summer (JJA; a, b) and autumn (SON; c, d). All fluxes are positive downward. The ice sheet is divided into three different zones: (i) the accumulation zone, (ii) the percolation zone, and (iii) the ablation zone.

In summary, our analysis highlights that Greenland is losing more mass in CMIP6 due to two factors:

1. a (known) greater sensitivity to greenhouse gas emissions and therefore warmer temperatures
2. previously unnotified cloud-related surface energy budget changes between CMIP5 and CMIP6 that enhance the GrIS sensitivity to warming.

Code and data availability. We provide examples of the Python code used to analyse the MAR model results. The code can be found at <https://doi.org/10.5281/zenodo.10462672> (Mostue, 2023). All the MAR model results are available for download on <http://phyc15.geo.ulg.ac.be/fettweis/MARv3.9/ISMIP6/> in the framework of the ISMIP6 exercise (<https://doi.org/10.5194/tc-14-2331-2020>, Nowicki et al., 2020). CMIP5 and CMIP6 model outputs can be openly accessed via different ESGF data nodes (e.g. <https://esgf-node.ipsl.upmc.fr/projects/cmip6-ipsl/>, IPSL, 2021, last access: 16 January 2024) (<https://esgf-node.ipsl.upmc.fr/projects/cmip5-ipsl/>, IMBIE2, 2020, last access: 16 January 2024).

Supplement. The supplement related to this article is available online at: <https://doi.org/10.5194/tc-18-475-2024-supplement>.

Author contributions. SH designed the study with contributions from IAM and TS. XF ran the MARv3.9 simulations and provided the outputs. IAM analysed all data, produced the figures, and prepared the paper. All authors discussed the results and were involved in editing the paper.

Competing interests. The contact author has declared that none of the authors has any competing interests.

Disclaimer. Publisher's note: Copernicus Publications remains neutral with regard to jurisdictional claims made in the text, published maps, institutional affiliations, or any other geographical representation in this paper. While Copernicus Publications makes every effort to include appropriate place names, the final responsibility lies with the authors.

Acknowledgements. The computations and simulations of this research were performed on resources provided by UNINETT Sigma2 – the national infrastructure for high-performance computing and data storage in Norway. The work of this study builds on the master's thesis of Mostue (2022).

Financial support. This research has been supported by the European Research Council (grant no. 758005) under the European Union's Horizon 2020 research and innovation programme.

Review statement. This paper was edited by Emily Collier and reviewed by two anonymous referees.

References

- Barthel, A., Agosta, C., Little, C. M., Hattermann, T., Jourdain, N. C., Goelzer, H., Nowicki, S., Seroussi, H., Straneo, F., and Bracegirdle, T. J.: CMIP5 model selection for ISMIP6 ice sheet model forcing: Greenland and Antarctica, *The Cryosphere*, 14, 855–879, <https://doi.org/10.5194/tc-14-855-2020>, 2020.
- Bennartz, R., Shupe, M. D., Turner, D. D., Walden, V. P., Steffen, K., Cox, C. J., Kulie, M. S., Miller, N. B., and Pettersen, C.: July 2012 Greenland melt extent enhanced by low-level liquid clouds, *Nature*, 496, 83–86, <https://doi.org/10.1038/nature12002>, 2013.
- Box, J. E., Fettweis, X., Stroeve, J. C., Tedesco, M., Hall, D. K., and Steffen, K.: Greenland ice sheet albedo feedback: thermodynamics and atmospheric drivers, *The Cryosphere*, 6, 821–839, <https://doi.org/10.5194/tc-6-821-2012>, 2012.
- Box, J. E., Wehrlé, A., van As, D., Fausto, R. S., Kjeldsen, K. K., Dachauer, A., Ahlstrøm, A. P., and Picard, G.: Greenland Ice Sheet Rainfall, Heat and Albedo Feedback Impacts From the Mid-August 2021 Atmospheric River, *Geophys. Res. Lett.*, 49, <https://doi.org/10.1029/2021GL097356>, 2022.
- Brun, E., David, P., Sudul, M., and Brunot, G.: A numerical model to simulate snow-cover stratigraphy for op-

- erational avalanche forecasting, *J. Glaciol.*, 38, 13–22, <https://doi.org/10.3189/S002214300009552>, 1992.
- Charalampidis, C., van As, D., Box, J. E., van den Broeke, M. R., Colgan, W. T., Doyle, S. H., Hubbard, A. L., MacFerrin, M., Machguth, H., and Smeets, C. J. P. P.: Changing surface–atmosphere energy exchange and refreezing capacity of the lower accumulation area, West Greenland, *The Cryosphere*, 9, 2163–2181, <https://doi.org/10.5194/tc-9-2163-2015>, 2015.
- De Ridder, K.: The Impact of Vegetation Cover on Sahelian Drought Persistence, *Bound.-Lay. Meteorol.*, 88, 307–321, <https://doi.org/10.1023/A:1001106728514>, 1998.
- Delhasse, A., Kittel, C., Amory, C., Hofer, S., van As, D., S. Fausto, R., and Fettweis, X.: Brief communication: Evaluation of the near-surface climate in ERA5 over the Greenland Ice Sheet, *The Cryosphere*, 14, 957–965, <https://doi.org/10.5194/tc-14-957-2020>, 2020.
- Doblas-Reyes, F. J., Sörensson, A. A., Almazroui, M., Dosio, A., Gutowski, W. J., Haarsma, R., Hamdi, R., Hewitson, B., Kwon, W.-T., Lamptey, B. L., Maraun, D., Stephenson, T. S., Takayabu, I., Terray, L., Turner, A., and Zuo, Z.: Linking Global to Regional Climate Change, in *Climate Change 2021: The Physical Science Basis. Contribution of Working Group I to the Sixth Assessment Report of the Intergovernmental Panel on Climate Change*, edited by: Masson-Delmotte, V., Zhai, P., Pirani, A., Connors, S. L., Péan, C., Berger, S., Caud, N., Chen, Y., Lonnoy, L., Goldfarb, M. I. Gomis, M., Huang, K., Leitzell, E., Matthews, J. B. R., Maycock, T. K., Waterfield T., Yelekçi, O., Yu, R., and Zhou, B., Cambridge University Press, Cambridge, United Kingdom and New York, NY, USA, 1363–1512, <https://doi.org/10.1017/9781009157896.012>, 2021.
- Fausto, A. D., Box, J. E., Colgan, W., Langen, P. L., and Mottram, R. H.: The implication of nonradiative energy fluxes dominating Greenland ice sheet exceptional ablation area surface melt in 2012, *Geophys. Res. Lett.*, 43, <https://doi.org/10.1002/2016GL067720>, 2016.
- Fettweis, X., Tedesco, M., van den Broeke, M., and Ettema, J.: Melting trends over the Greenland ice sheet (1958–2009) from spaceborne microwave data and regional climate models, *The Cryosphere*, 5, 359–375, <https://doi.org/10.5194/tc-5-359-2011>, 2011.
- Fettweis, X., Franco, B., Tedesco, M., van Angelen, J. H., Lenaerts, J. T. M., van den Broeke, M. R., and Gallée, H.: Estimating the Greenland ice sheet surface mass balance contribution to future sea level rise using the regional atmospheric climate model MAR, *The Cryosphere*, 7, 469–489, <https://doi.org/10.5194/tc-7-469-2013>, 2013.
- Fettweis, X., Box, J. E., Agosta, C., Amory, C., Kittel, C., Lang, C., van As, D., Machguth, H., and Gallée, H.: Reconstructions of the 1900–2015 Greenland ice sheet surface mass balance using the regional climate MAR model, *The Cryosphere*, 11, 1015–1033, <https://doi.org/10.5194/tc-11-1015-2017>, 2017.
- Franco, B., Fettweis, X., and Ericpic, M.: Future projections of the Greenland ice sheet energy balance driving the surface melt, *The Cryosphere*, 7, 1–18, <https://doi.org/10.5194/tc-7-1-2013>, 2013.
- Gallee, H. and Schayes, G.: Development of a three-dimensional meso- γ primitive equation model: katabatic winds simulation in the area of Terra Nova Bay, Antarctica, *Mon. Weather Rev.*, 122, 671–685 [https://doi.org/10.1175/1520-0493\(1994\)122<0671:DOATDM>2.0.CO;2](https://doi.org/10.1175/1520-0493(1994)122<0671:DOATDM>2.0.CO;2), 1994.
- Hanna, Huybrechts, P., Steffen, K., Cappelen, J., Huff, R., Shuman, C., Irvine-Fynn, T., Wise, S., and Griffiths, M.: Increased Runoff from Melt from the Greenland Ice Sheet, *J. Climate*, 21, 331–341, <https://doi.org/10.1175/2007JCLI1964.1>, 2008.
- Hansen, N., Simonsen, S. B., Boberg, F., Kittel, C., Orr, A., Souverijns, N., van Wessem, J. M., and Mottram, R.: Brief communication: Impact of common ice mask in surface mass balance estimates over the Antarctic ice sheet, *The Cryosphere*, 16, 711–718, <https://doi.org/10.5194/tc-16-711-2022>, 2022.
- Hauer, Fussell, E., Mueller, V., Burkett, M., Call, M., Abel, K., McLeman, R., and Wrathall, D.: Sea-level rise and human migration, *Nat. Rev. Earth Environ.*, 1, 28–39, <https://doi.org/10.1038/s43017-019-0002-9>, 2020.
- Hofer, S., Tedstone, A. J., Fettweis, X., and Bamber, J. L.: Decreasing cloud cover drives the recent mass loss on the Greenland Ice Sheet, *Sci. Adv.*, 3, e1700584–e1700584, <https://doi.org/10.1126/sciadv.1700584>, 2017.
- Hofer, S., Tedstone, A. J., Fettweis, X., and Bamber, J. L.: Cloud microphysics and circulation anomalies control differences in future Greenland melt, *Nat. Clim. Change*, 9, 523–528, <https://doi.org/10.1038/s41558-019-0507-8>, 2019.
- Hofer, S., Lang, C., Amory, C., Kittel, C., Delhasse, A., Tedstone, A., and Fettweis, X.: Greater Greenland Ice Sheet contribution to global sea level rise in CMIP6, *Nat. Commun.*, 11, 6289, <https://doi.org/10.1038/s41467-020-20011-8>, 2020.
- IMBIE2: Mass balance of the Greenland Ice Sheet from 1992 to 2018, *Nature*, 579, 233–239, <https://doi.org/10.1038/s41586-019-1855-2>, 2020.
- IPSL, France: CMIP5 @ IPSL [data set], <https://esgf-node.ipsl.upmc.fr/projects/cmip5-ipsl/> (last access: 16 January 2024), 2021a.
- IPSL, France: WCRP Coupled Model Intercomparison Project (Phase 6), [data set], <https://esgf-node.ipsl.upmc.fr/projects/cmip6-ipsl/> (last access: 16 January 2024), 2021b.
- Kjeldsen, Khan, S. A., Colgan, W. T., MacGregor, J., and Fausto, R. S.: Time-Varying Ice Sheet Mask: Implications on Ice-Sheet Mass Balance and Crustal Uplift, *J. Geophys. Res.-Earth*, 125, <https://doi.org/10.1029/2020JF005775>, 2020.
- Lefebvre, Gallée, H., van Ypersele, J.-P., and Greuell, W.: Modeling of snow and ice melt at ETH Camp (West Greenland): A study of surface albedo, *J. Geophys. Res.*, 108, 4231, <https://doi.org/10.1029/2001JD001160>, 2003.
- McCrystall, Stroeve, J., Serreze, M., Forbes, B. C., and Screen, J. A.: New climate models reveal faster and larger increases in Arctic precipitation than previously projected, *Nat. Commun.*, 12, 6765–12, <https://doi.org/10.1038/s41467-021-27031-y>, 2021.
- Mostue, I. A.: Greenland Surface Energy Budget Response in CMIP6 (Master Thesis), University of Oslo, <http://urn.nb.no/URN:NBN:no-96440> (last access: August 2022), 2022.
- Mostue, I. A.: MAR CMIP5 CMIP6 analysis, Zenodo [code], <https://doi.org/10.5281/zenodo.10462672>, (last access: 16 January 2024), 2023.
- Mouginot, J., Rignot, E., Björk, A., van den Broeke, M., Milan, R., Morlighem, M., Noël, B., Scheuchl, B., and Wood, M.: Forty-six years of Greenland Ice Sheet mass balance from 1972 to 2018, *P. Natl. Acad. Sci. USA*, 116, 9239–9244, <https://doi.org/10.1073/pnas.1904242116>, 2019.
- Nowicki, S., Goelzer, H., Seroussi, H., Payne, A. J., Lipscomb, W. H., Abe-Ouchi, A., Agosta, C., Alexander, P., Asay-Davis, X.

- S., Barthel, A., Bracegirdle, T. J., Cullather, R., Felikson, D., Fettweis, X., Gregory, J. M., Hattermann, T., Jourdain, N. C., Kuipers Munneke, P., Larour, E., Little, C. M., Morlighem, M., Nias, I., Shepherd, A., Simon, E., Slater, D., Smith, R. S., Straneo, F., Trusel, L. D., van den Broeke, M. R., and van de Wal, R.: Experimental protocol for sea level projections from ISMIP6 stand-alone ice sheet models, [data set] *The Cryosphere*, 14, 2331–2368, <https://doi.org/10.5194/tc-14-2331-2020>, 2020.
- Noël, B., Berg, W. J. van de, Lhermitte, S. and Broeke, M. R. van den.: Rapid ablation zone expansion amplifies north Greenland mass loss, *Sci. Adv.*, 5, <https://doi.org/10.1126/sciadv.aaw0123>, 2019.
- Noël, van Kampenhout, L., Lenaerts, J. T. M., van de Berg, W. J., and van den Broeke, M. R.: A 21st Century Warming Threshold for Sustained Greenland Ice Sheet Mass Loss, *Geophys. Res. Lett.*, 48, <https://doi.org/10.1029/2020GL090471>, 2021.
- O'Neill, B. C., Tebaldi, C., van Vuuren, D. P., Eyring, V., Friedlingstein, P., Hurtt, G., Knutti, R., Krieglner, E., Lamarque, J.-F., Lowe, J., Meehl, G. A., Moss, R., Riahi, K., and Sanderson, B. M.: The Scenario Model Intercomparison Project (ScenarioMIP) for CMIP6, *Geosci. Model Dev.*, 9, 3461–3482, <https://doi.org/10.5194/gmd-9-3461-2016>, 2016.
- Screen, J. A. and Simmonds, I.: The central role of diminishing sea ice in recent Arctic temperature amplification, *Nature*, 464, p.1334–1337, <https://doi.org/10.1038/nature09051>, 2010.
- Shupe, M. D. and Intrieri, J. M.: Cloud Radiative Forcing of the Arctic Surface: The Influence of Cloud Properties, Surface Albedo, and Solar Zenith Angle, *J. Climate*, 17, 616–628, [https://doi.org/10.1175/1520-0442\(2004\)017<0616:CRFOTA>2.0.CO;2](https://doi.org/10.1175/1520-0442(2004)017<0616:CRFOTA>2.0.CO;2), 2004.
- Tedesco, Fettweis, X., van den Broeke, M. R., van de Wal, R. S. W., Smeets, C. J. P. P., van de Berg, W. J., Serreze, M. C., and Box, J. E.: The role of albedo and accumulation in the 2010 melting record in Greenland, *Environ. Res. Lett.*, 6, 014005, <https://doi.org/10.1088/1748-9326/6/1/014005>, 2011.
- Tedesco, Mote, T., Fettweis, X., Hanna, E., Jeyaratnam, J., Booth, J. F., Datta, R., and Briggs, K.: Arctic cut-off high drives the poleward shift of a new Greenland melting record, *Nat. Commun.*, 7, 11723–11723, <https://doi.org/10.1038/ncomms11723>, 2016.
- Van de Wal, R. S. W., Greuell, W., van den Broeke, M. R., Reijmer, C. H., Oerlemans, J., Willis, I. C., and Dowdeswell, J.: Surface mass-balance observations and automatic weather station data along a transect near Kangerlussuaq, West Greenland, *Ann. Glaciol.*, 42, 311–316, 2005.
- van den Broeke, M. R., Smeets, C. J. P. P., and van de Wal, R. S. W.: The seasonal cycle and interannual variability of surface energy balance and melt in the ablation zone of the west Greenland ice sheet, *The Cryosphere*, 5, 377–390, <https://doi.org/10.5194/tc-5-377-2011>, 2011.
- van den Broeke, M., Smeets, P., Ettema, J., and Munneke, P. K.: Surface radiation balance in the ablation zone of the west Greenland ice sheet, *J. Geophys. Res.-Atmos.*, 113, D13105, <https://doi.org/10.1029/2007JD009283>, 2008.
- van den Broeke, M. R., Enderlin, E. M., Howat, I. M., Kuipers Munneke, P., Noël, B. P. Y., van de Berg, W. J., van Meijgaard, E., and Wouters, B.: On the recent contribution of the Greenland ice sheet to sea level change, *The Cryosphere*, 10, 1933–1946, <https://doi.org/10.5194/tc-10-1933-2016>, 2016.
- van den Broeke, M., Box, J., Fettweis, X., Hanna, E., Noël, B., Tedesco, M., van, As, D., Berg, W. J., and van de Kampenhout, L.: Greenland Ice Sheet Surface Mass Loss: Recent Developments in Observation and Modeling, *Curr. Clim. Change Rep.*, 3, 345–356, <https://doi.org/10.1007/s40641-017-0084-8>, 2017.
- van Tricht, K. et al.: Clouds enhance Greenland ice sheet meltwater runoff, *Nat. Commun.*, 7, 10266, <https://doi.org/10.1038/ncomms10266>, 2016.
- Vionnet, V., Brun, E., Morin, S., Boone, A., Faroux, S., Le Moigne, P., Martin, E., and Willemet, J.-M.: The detailed snowpack scheme Crocus and its implementation in SURFEX v7.2, *Geosci. Model Dev.*, 5, 773–791, <https://doi.org/10.5194/gmd-5-773-2012>, 2012.